Highly sensitive organic thin-film transistors based sensor for putrescine detection

Jiaxin Zhu[1] · **Xiao Wang**[1] · **Haizeng Wang**[1,2]

Abstract

Organic thin-film transistor (OTFT) sensors based on a diketopyrrolopyrrole–thiophene polymer (PDQT) were fabricated to detect putrescine (PUT) vapors in air. Electrical properties and film characteristics of the sensors were examined with IV characterization, AFM and XRD. Upon PUT exposure, PDQT sensors showed fast responses and quick recovery. Two groups of sensors with different active layer thickness were compared for stability and sensitivity. Although with less stability under ambient conditions, sensors with thinner layers showed high sensitivity toward PUT with detection limit of 3 ppb. The group with thicker layers exhibited ideal long-term stability through 8 weeks of air storage along with proper reusability and reproducibility. The PDQT sensors showed a selectivity toward ammonia and biogenic amines. A preliminary test with food samples was carried out where PDQT sensors gave promising responses toward food-emitted vapors. Such sensors might be used in real-time freshness monitoring with further modification to lower the operational voltage and improve the stability.

Keywords OTFT · Putrescine · Diketopyrrolopyrrole polymer · Air stable · Spoilage detection

1 Introduction

Organic thin-film transistors (OTFTs) as typical modern electronics have been highly developed and employed into various applications in recent years [1–3]. Compared with their inorganic counterparts, OTFTs use a wide range of organic semiconductors that allow low-temperature processes along fabrication. Conventional metal-based sensors are known to be sensitive and stable toward many analytes; however, organic transistors hold better bio-compatibility which allow them to be used in biosensing applications. In addition to multi-parameter producibility, flexibility and

improved sensitivity and stability, OTFTs have shown the potential to exceed inorganic devices in the sensing area [4]. A diverse range of OTFT sensors have been reported in recent years aiming at different analytes [5–7]. The target analytes have been mainly focused on nitrogen dioxide, hydrogen sulfide and ammonia. There were few studies of OTFTs sensing on biogenic amines in vapors and aqueous solutions, but none has set putrescine as main analyte for sensing [8–10].

Putrescine (PUT), also known as 1,4-diaminobutane or butanediamine, is mostly produced through polyamine metabolism in cell proliferation and organism growth as an intermediate [11]. In addition, PUT can be massively released by spoilage from manifold food products especially fermented ones [12, 13]. It was proven that health issues could be aroused with high consumption of PUT in a short time [14, 15]. In food industry, PUT has been used as quality index in food productions, and employed as one of the most important indicators of food spoilage [16, 17]. PUT detection is usually based on laborious analysis with HPLC, GC, UV, etc. However, such methods need complicated sample pretreatment and buffer preparation which consumes long time [18–20]. There have been several techniques and methods including near field communication (NFC) technology,

✉ Jiaxin Zhu
jancyzhu@outlook.com

1 Key Laboratory of Marine Chemistry Theory and Technology, Ministry of Education, College of Chemistry and Chemical Engineering, Ocean University of China, Qingdao 266100, China

2 Shandong Key Laboratory of Marine Fine Chemicals, Shandong Ocean Chemical Industry Scientific Research Institute, Weifang 262737, China

protein-based biosensor and molecular imprinting technique to be used in the detection of PUT [17, 21, 22].

Since 2005, diketopyrrolopyrrole (DPP)-based polymers have been broadly investigated for OTFT applications due to their remarkable properties of charge transport and air stability [23, 24]. In gas sensing area, OTFTs-based sensors with DPP polymers exhibited high sensitivity and ideal stability for detection of many inorganic gaseous analytes as well as several organic compounds [25]. In this paper, we report an OTFT sensor based on a diketopyrrolopyrrole polymer poly[2,5-bis(2-octyldodecyl)pyrrolo-[3,4-c]pyrrole-1,4(2H,5H)-dione-alt-2,2′:5′,2″:5″,2′′′-quaterthi-ophene] (PDQT) to detect PUT vapors. Two groups of sensors were made with different active layer thickness. Stability of both groups was investigated, where the sensors with thicker layers showed better stability among 8 weeks of storage. Fast responses and recovery were observed for the PDQT sensors upon exposure to PUT vapors from 0 to 100 ppm. Sensitivity of the sensors was evaluated with current relative responses as a function of exposed PUT concentrations. Limit of detection (LOD) was found at 13 ppm with the thicker-layer sensors and 3 ppb with the thinner-layer sensors. Selectivity of the sensor was investigated with acetone, ethanol, toluene, cadaverine and ammonia. The PDQT sensors showed a satisfied discrimination toward ammonia and biogenic amines. To further explore the potential in practical freshness monitoring, food-emitted vapors were used to test sensibility of the PDQT sensors. Responses of the sensors met the expectation in detection of vapors emitted from food samples stored for 1–3 days.

2 Experimental section

2.1 Fabrication and characterization

Poly[2,5-bis(2-octyldodecyl)pyrrolo-[3,4-c]pyrrole-1,4(2H,5H)-dione-alt-2,2′:5′,2″:5″,2′′′-quaterthiophene] was prepared by Stille coupling following the synthesis route reported by Ha et al. [26]. Structure and energy levels of PDQT are presented in Fig. 1. Number average and weight average molecular weight of PDQT were measured with gel permeation chromatography (GPC) at 150 °C with 1,2,4-trichlorobenzene as eluent and polystyrenes as standard. ^{1}H NMR spectra were measured on a Bruker AVANCE III 400 MHz spectrometer in CDCl$_3$, and the chemical shifts were referenced to internal tetramethylsilane (TMS).

Bottom-gate, bottom-contact OTFT devices were fabricated on heavily n^{++}-doped silicon wafers with ~300 nm thermally grown SiO$_2$ top layer (capacitance of ~11 nF cm^2). Gold source and drain patterns were deposited by thermal evaporation on the SiO$_2$ layer using a conventional lithography technique. The device
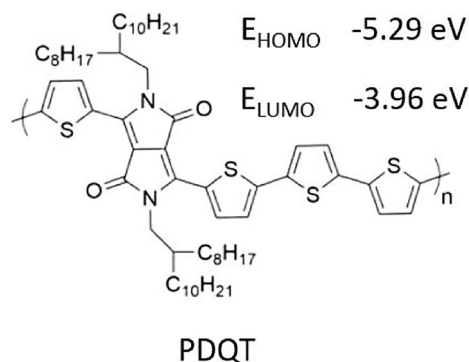

Fig. 1 Chemical structure and energy level of PDQT

dimensions of the PDQT transistors were $W = 15,800$ μm, $L = 30$ μm. Transistors were sonicated with acetone and 2-propanol for 20 min, respectively, to remove oxidized gold and carbonaceous residues. Then, an air plasma treatment was carried out for 2 min, followed with ethanol and chloroform cleaning. Octane-thiol (ODT) treatment with 10 mM ODT in ethanol solution was used afterwards, to form self-assembled monolayers on gold. Subsequently, a dodecyltrichlorosilane modification was used to form self-assembled monolayers on the dielectric layer. The OTFT devices were then washed by toluene and dried out in the glovebox (argon).

Thin layers of PDQT were spin-coated on the cleaned transistors in the glovebox with 5 mg/mL polymer solutions in chloroform. Subsequently, thermal annealing was carried out at 150 °C in the glovebox (argon). The regular PDQT sensors were fabricated at spin-coating speed of 3000 rpm and annealed for 30 min. A group B of PDQT sensors were fabricated at spin-coating speed of 4000 rpm and annealed for 1 h. Film thickness and quality were examined by atomic force microscopy (AFM) with a dimension 3100 scanning probe microscope. X-ray diffraction patterns were obtained using a Bruker D8 Advance Discover diffractometer with Cu Kα radiation ($\lambda = 1.5418$ Å). At least 5 devices were tested from each batch of the fabricated transistors.

Agilent B2912A source measurement unit analyzer was used for sensors characterization and sensing evaluations. Field-effect mobility of the PDQT sensor was calculated in the saturated region of the transfer curve according to Eq. 1:

$$I_{DS} = \mu \frac{CW}{2L} \cdot (V_{GS} - V_{TH})^2 \tag{1}$$

where I_{DS} is the drain–source current. μ is the field-effect charge mobility of the device. C is the gate dielectric capacitance per unit area. W is the channel width, and L is the channel length of the device. V_{GS} is the gate voltage. V_{TH} is the threshold voltage.

2.2 Sensing evaluation

All vapors were prepared by controllably dilution with dry air and presented in analyte volume/air volume (v/v) form. Electrical properties of the PDQT sensors were characterized before and after PUT vapor exposure. To obtain real-time responses of the sensor, I_{DS} versus time measurement was used at operational $V_{GS} = V_{DS} = -100$ V. Response time of the sensor was calculated as the time period between vapor injection and 90% of current changes caused by gas exposure. Relative response of the sensor was calculated by the following equations:

$$I_{DS} \text{ fraction (diluted PUT)} = \Delta I_{DS} \text{ (gas inject)} \Big/ \Delta I_{DS} \text{(pristine)}$$

$$= \frac{I_{DS}(T_2) - I_{DS}(T_1)}{T_2 - T_1} \Big/ \frac{I_{DS}(T_1) - I_{DS}(T_0)}{T_1 - T_0} \tag{2}$$

$$\text{Relative response (\%)} = I_{DS} \text{ fraction}$$
$$\text{(diluted PUT)} \Big/ I_{DS} \text{ fraction (saturated PUT)} \times 100\% \tag{3}$$

where T_1 was the time when analyte was injected. T_2 was the time when current reached to 90% of the largest extent caused by vapor exposure. ($T_1 - T_0 = T_2 - T_1 =$ response time)

Sensitivity of the sensors was evaluated by plotting relative responses and signal to noise ratio (SNR) as a function of PUT concentration, where SNR was extracted from the I_{DS} versus time plots. Limit of detection (LOD) was determined as the PUT vapor concentration when SNR = 3.

3 Results and discussion

3.1 Transistor characterization

^{1}H NMR of the PDQT is shown in Figure S1. Number average molecular weight (M_n) of PDQT was measured to be 20 kg mol^{-1} and weight average molecular weight (M_w) was 51 kg mol^{-1}. PDQT thin films of the sensors were characterized with AFM. As shown in Fig. 2a, a bush-like surface of PDQT thin layer with small "gaps" can be seen with the sensor with regular layer thickness. Distributions of these small "gaps" are quite even to produce a smooth and continuous layer of PDQT which facilitated charge transport and gas adsorption. Between two groups of PDQT sensors with different layer thickness, surface of the regular sensors showed a higher degree of roughness with larger grains (Figure S2a). Layer thickness of the group B sensors was measured as ~25 nm, which was 4 nm thinner than the regular sensors that gave better smoothness of the active films (Figure S2b). Average layer thickness of the PDQT OTFT devices without PUT exposure was around 29 nm (measured by 10 devices). With PUT vapor exposure, PDQT films got thicker. As shown in Fig. 2b and c, the PDQT sensor exposed to dry PUT vapor showed only slight increase of layer thickness and higher degree of roughness, while wet

Fig. 2 **a** 3D AFM image of the PDQT film without PUT exposure. Layer thickness = 29 nm. R_q = 0.458 nm. **b** AFM image of the PDQT film exposed to dry putrescine vapor (75 ppm). Layer thickness = 30 nm. R_q = 0.464 nm. **c** AFM image of the PDQT film exposed to wet putrescine vapor (75 ppm). Layer thickness = 34 nm. R_q = 0.455 nm. [regular sensors]
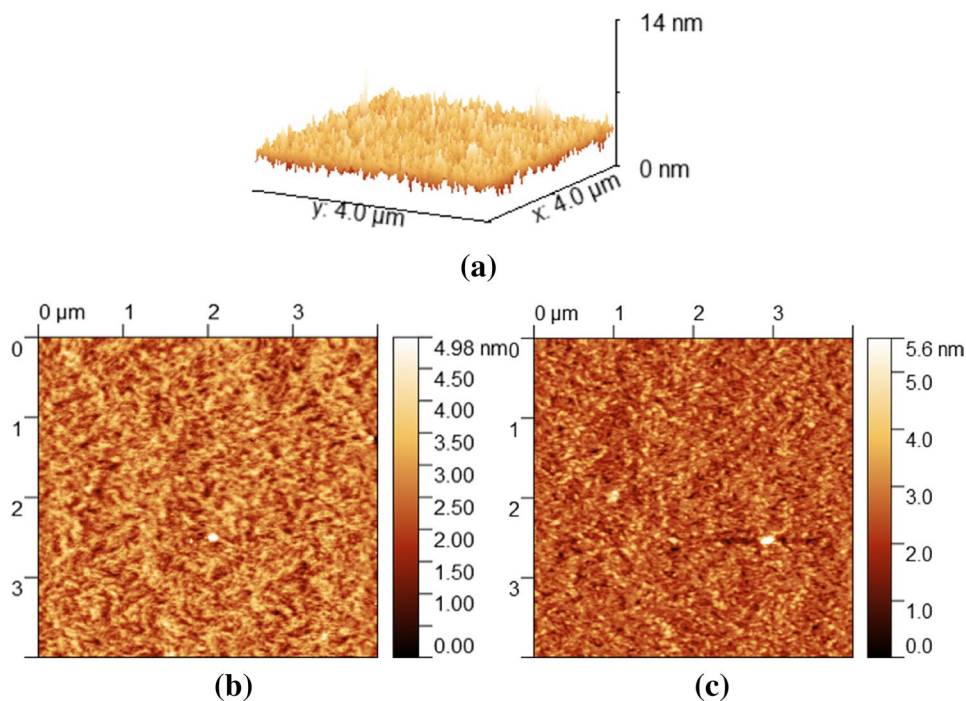
PUT exposure caused an additional increase of layer thickness but smoothened the surface of PDQT.

Electrical properties of the PDQT sensors are listed in Table S1. An enhancement of mobility was observed when tested the sensors in air compared to which in argon, which was possibly ascribed to the oxygen in air that interacted with the golden contacts to lower the hole injection barrier [27]. On the other hand, moisture in air showed a small effect on charge transport of the PDQT devices as shown in Table S1. As mentioned before, semiconducting layer thickness of the sensor got increased by 5 nm with wet PUT vapor exposure. Compared with the film exposed to dry PUT, such increase of thickness was likely due to the adsorption of water molecules, whereas, according to transistor parameters, water adsorption showed only small effect on charge transport of the sensor. Transistor performance of the sensors in group B was significantly poorer than the regular ones. Mobility of this group of devices was less than half of the regular ones. In addition, V_{TH} of these sensors was much larger as well. $I_{on/off}$ of the group B devices was only reached 10^3. Although mobility of the OTFT devices generally increases with thinner active layers, it has been reported that bias stress effect would be increased at lower thickness which would affect charge transport and cause shifts of V_{TH} [28]. In this study, spin-coating speed of the coating process has been set from 1000 to 5000 rpm. From 1000 to 3000 rpm, mobility of the devices showed a tendency of increase. However, with higher spinning speeds, mobility of the devices decreased severely. The highest mobility of the regular PDQT sensors was 0.304 cm^2 V^{-1} s^{-1} in air (Fig. 3a and b). Reproducible results were observed with devices made from more than 10 batches. Upon exposure to 20 ppm PUT, PDQT sensor showed a prompt mobility decrease along with threshold voltage shifted negatively (Fig. 3c and d). But after 30 s of PUT injection, mobility of the sensor recovered nearly 88% and V_{TH} recovered over 90% (Figure S3).

3.2 Sensing properties

For practical applications, stability is an important aspect to be fulfilled. In this study, storage stability as well as operational stability was evaluated. Storage stability of PDQT sensors was evaluated with mobility changes of the devices. Long-term air stability of the regular PDQT devices showed a total drop of mobility less than 12% over 8 weeks of storage (Fig. 4a). Upon weekly exposure to PUT vapors (20 ppm), mobility of the regular sensors showed a relatively large decline when stored in argon, while less decline was seen when stored in air (Fig. 4b). For the sensors in group B, much degradation was observed within only 4 weeks of storage (Figure S4), which demonstrated poor stability.

Operational stability of the PDQT sensors was evaluated by measuring I_{DS} along time under continuous bias. As shown in Fig. 4c, the sensor showed current degradation with constant bias set at −100 V. After ~10 s of PUT vapor exposure, I_{DS} of the sensor showed a nearly linear decreasing trend. By PUT exposure, current of the sensor decreased to a significant extent. With an extended period of time, current of the PDQT device gradually recovered to ~80% of the original level. It has been noticed that for the OTFT devices, operational stability would be significantly affected by oxygen and water molecules in ambient conditions combined with large operation power density [29, 30].

I_{DS} drops of the sensors were observed in the real-time detection tests as well (Fig. 5a). Despite the abovementioned current degradation, I_{DS} flows along time under continuous bias made it easy to show the real-time responses of the sensors when exposed to target analytes. As shown in Fig. 5a, regular PDQT sensors gave fast responses toward PUT vapors injection. The average response time arrived at around 2 s for over 10 devices. Relative responses which were calculated from I_g/I_0 showed an s-shape response curve of the sensor exposing to the increased concentrations of PUT (Fig. 5b). Repeating gas sensing tests were carried out with 5 devices to be daily exposed to 45 ppm PUT vapors for 5 days. Responses with an average deviation of 1.5 were seen, which proved the reproducibility and reusability of the PDQT sensors (Figure S5a). Repeatable responses were observed in the multiple exposure tests on the same device as well (Figure S5b). Responses of the sensor showed that upon exposure to PUT vapors over 75 ppm, current of the sensors got instantly saturated, which suggested the maximum detectable concentration of PUT for the PDQT sensors to be 75 ppm. Limit of detection for the regular PDQT sensor was found at 13 ppm (SNR = 3) (Fig. 5b).

Compared with the regular PDQT sensors, group B devices with thinner active layers exhibited an ultra-high sensitivity (Fig. 5c). Ppb-level of the PUT vapors were successfully detected. LOD of this group of sensors reached 3 ppb (SNR = 3), which was close to detection limit of the fluorescent sensors reported by Hu et al. (LOD = 2.6 ppb) and surpassed the NFC sensors presented by Ma et al. (LOD = 5 ppm) in 2018 [17, 31]. For OTFT-based sensors, it was proved that thinner active layers would lead to a better sensitivity [32]. In spite of its poor environmental stability, this group of thinner-layer sensors showed higher sensitivity toward PUT vapors. Proper way of encapsulation might be applied in the future to allow better stability of such highly sensitive sensors to be used in practical applications.

To investigate selectivity of the regular PDQT sensors, 5 vaporous analytes were tested in addition to PUT (Fig. 6). I_{DS} reduction was observed upon exposure to these 5 types of vapors. Non-amine analytes including acetone, ethanol
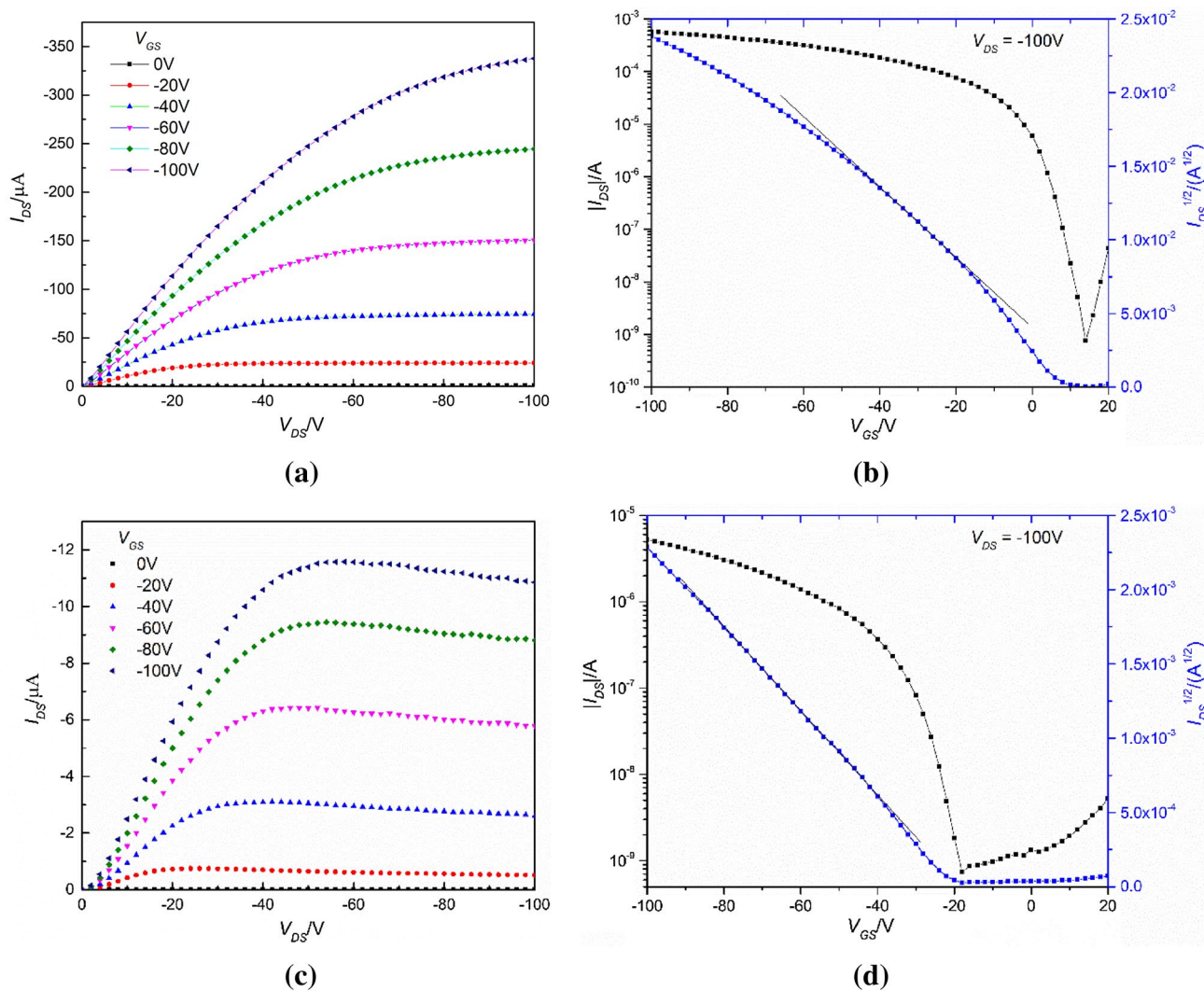
Fig. 3 **a** Output and **b** transfer characteristics of the PDQT sensor without PUT exposure; **c** output and **d** transfer characteristics of the PDQT sensor after exposure to 20 ppm PUT

and toluene, were made into 75 and 200 ppm vapors to test on PDQT sensors (Figure S6a). Only small responses were observed by 200 ppm exposure of acetone and toluene. For ethanol vapors, no response was recorded. On the other hand, 45 ppm of cadaverine (CAD) and ammonia caused significant responses of the sensor. Compared with PUT, responses toward cadaverine with the same concentration were lower, while the responses toward ammonia were around the same level with PUT (Figure S6b and c). Therefore, the PDQT sensor showed a selectivity toward NH_3 and biogenic amines against non-amine vapors.

AFM images of the PDQT films exposed to acetone, ethanol and toluene are presented in Figure S7. Compared to the film exposed to dry PUT vapor (Fig. 2b), PDQT layers exposed to non-amine analytes showed lower roughness and similar impact in thickness changes. As shown in the XRD patterns in Figure S8, *d*-spacing of PDQT sensors exposed to any vapors was calculated to be 1.99 nm (by Bragg's Law). Combined with AFM and gas sensing results, crystallinity changes of the devices were possibly induced by moisture adsorption. Upon PUT injection, lone pairs of electrons which might interact with thiophene could trap the charges across the channel to increase trap charge density on the interface of semiconductor/dielectric [33]. Such trapping or de-doping effect was reflected in the negative V_{TH} shifts in the PDQT sensors when exposed to PUT. The trapped charges hindered the flow of free hole charges which resulted in current decreases and mobility drops of the sensor. In addition, current flow of the PDQT sensor recovered to
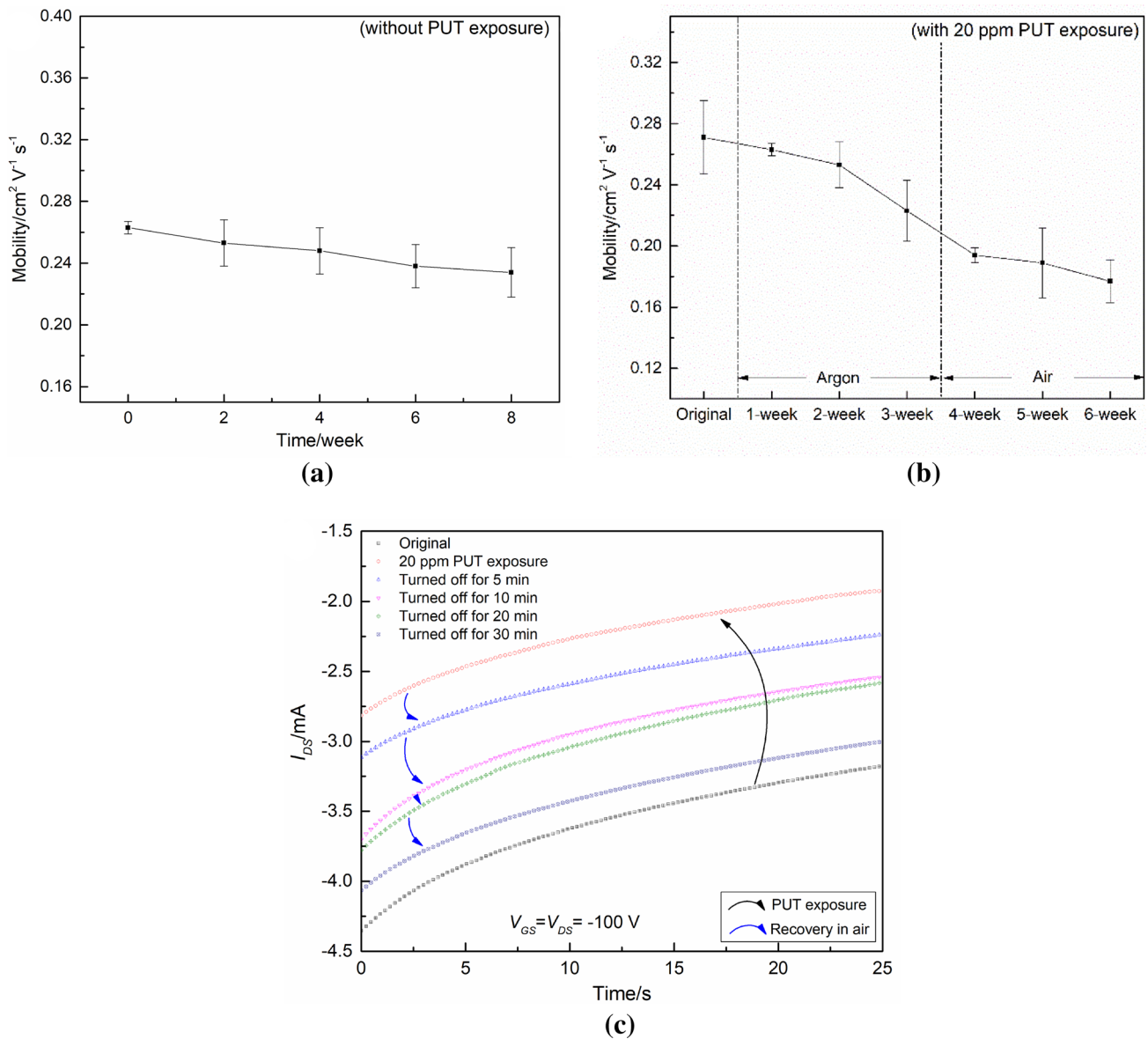
Fig. 4 **a** Mobility changes of the sensors stored in air. **b** Mobility changes of the sensors stored in argon and air upon weekly exposure to 20 ppm PUT. **c** I_{DS} flows of the sensors under constant bias. [regular sensors]

its original degrading tendency right after PUT injection, which likely indicated a weak physical absorption (Van der Waals force) of the PUT by PDQT. By sensing the ammonia and cadaverine, PDQT sensors gave a larger difference between CAD and PUT, and closer responses between PUT and NH_3, which indicated a relatively insignificant effect of basicity. The sensitivity differences among PUT, ammonia and cadaverine was likely due to the steric effect given the different sizes of these molecules.

Spoilage detection with food emitted vapors was attempted using peas, fish and chicken which were stored in the fridge and at room temperature (Figure S9). Increased responses were seen from the sensors with a prolonged storage time of food samples (Figure S10). For practical applications of the OTFT-based sensors, lower operating voltages and better stability are expected. To lower the drive voltage, gate materials with high dielectric constant can be used [34]. In addition, hybrid dielectrics might be employed to increase the capacitance per area (C) [35]. It has also been well proved that the decrease of film thickness would help to lower the operating voltage. In this study, PDQT sensors with thinner layers exhibited a high sensitivity but a lack of stability which might be induced by high operating voltages
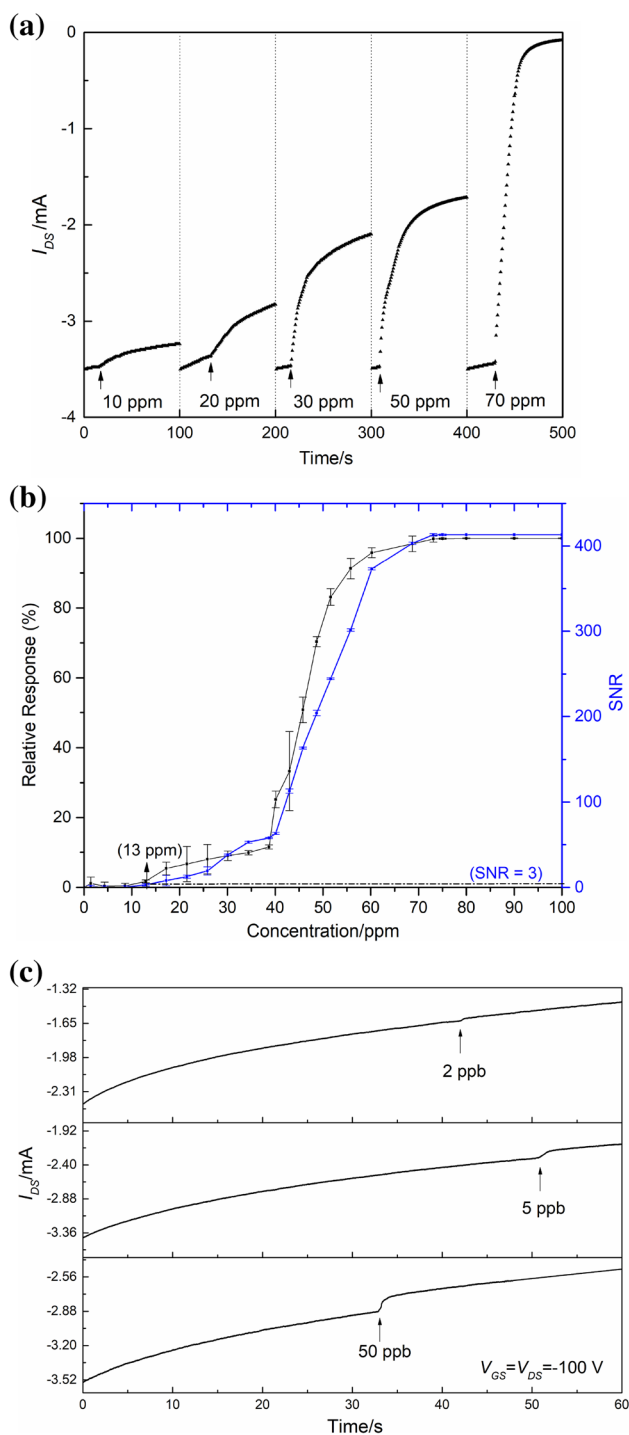
Fig. 6 Relative responses of the regular PDQT sensors toward different vapors (tested on 5 devices)

4 Conclusions

In summary, OTFT-based sensors with the diketopyrrolopyrrole–thiophene polymer PDQT were applied in real-time detection of PUT vapors under ambient conditions. An average response time of 2 s was realized in ambient operations. Detection limits reached 3 ppb with a group of sensors with thinner active layers. Sensors with thicker layers showed better stability along 8 weeks of air storage as well as ideal reusability. PDQT sensors showed significant selectivity toward PUT, CAD and ammonia against acetone, ethanol and toluene, which showed potential for such sensors to be used in freshness monitoring. Preliminary test on food emitted vapors was carried out, in which PDQT sensors gave promising responses. Device optimization with the addition of the encapsulation layer or modification of dielectrics can be applied to further improve sensing performance and lower the drive voltage for practical applications.

Compliance with ethical standards

Conflict of interest The authors declare no competing financial interest.

Fig. 5 a Real-time detection of the PUT vapors with different concentrations. **b** Relative responses of the sensors toward PUT vapors from 0 to 100 ppm.[regular sensors] **c** PDQT sensors with thinner layers sensing ppb levels of PUT vapors. [group B sensors]

[36]. To improve stability while applying lower drive voltage, proper encapsulation can be added to the devices with thinner layers.
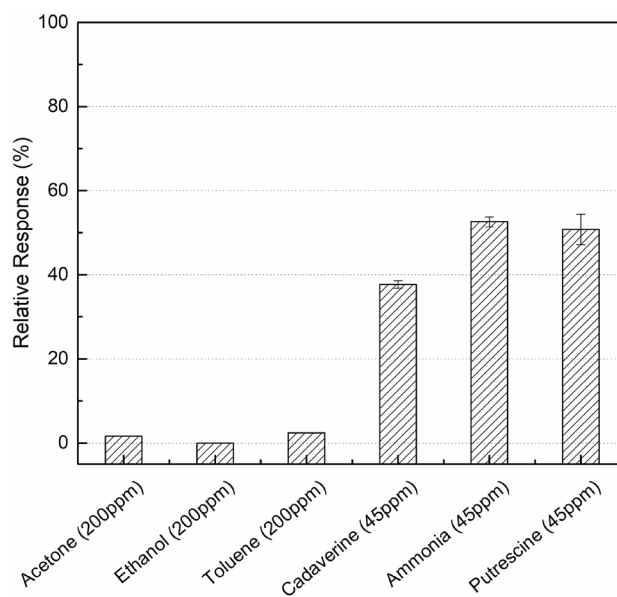
References

1. J. Lu, D. Liu, J. Zhou, Y. Chu, Y. Chen, X. Wu, J. Huang, Adv. Funct. Mater. **27**, 1700018 (2017)
2. T. Minami, Y. Sasaki, T. Minamiki, S. Wakida, R. Kurita, O. Niwa, S. Tokito, Biosens. Bioelectron. **81**, 87 (2016)
3. J.H.L. Ngai, L.M. Leung, S.K. So, H.K.H. Lee, Org. Electron. **32**, 258 (2016)
4. J. Yang, G. Xie, Y. Su, Q. Zhang, H. Du, H. Tai, X. Du, Y. Jiang, Sci. China Technol. Sci. **61**, 1696 (2018)
5. S. Hou, X. Zhuang, Z. Yang, J. Yu, Nanomaterials **8**, 203 (2018)
6. C. Zhang, P. Chen, W. Hu, Chem. Soc. Rev. **44**, 2087 (2015)
7. O. Knopfmacher, M.L. Hammock, A.L. Appleton, G. Schwartz, J. Mei, T. Lei, J. Pei, Z. Bao, Nat. Commun. **5**, 2954 (2014)
8. Y. Yang, G. Zhang, H. Luo, J. Yao, Z. Liu, D. Zhang, A.C.S. Appl. Mater. Interfaces **8**, 3635 (2016)
9. T. Minami, T. Sato, T. Minamiki, S. Tokito, Anal. Sci. **31**, 721 (2015)
10. L. Hague, D. Puzzovio, T.H. Richardson, M. Grell, Sens. Lett. **9**, 1692 (2011)
11. C.W. Tabor, H. Tabor, Microbiol. Rev. **49**, 81 (1985)
12. M.A. Rabie, H. Siliha, S. el-Saidy, A.-A. el-Badawy, F.X. Malcata, Innov. Food Sci. Emerg. Technol. **11**, 661 (2010)
13. H. Yu, S. Bo, Food Control **108**, 106861 (2019)
14. J.M. Poveda, Food Control **96**, 227 (2019)
15. A.R. Shalaby, Food Res. Int. **29**, 675 (1996)
16. M.R. Alberto, M.E. Arena, M.C. Manca de Nadra, Food Control **18**, 898 (2007)
17. Z. Ma, P. Chen, W. Cheng, K. Yan, L. Pan, Y. Shi, G. Yu, Nano Lett. **18**, 4570 (2018)
18. H. Zhai, X. Yang, L. Li, G. Xia, J. Cen, H. Huang, S. Hao, Food Control **25**, 303 (2012)
19. S. Köse, S. Koral, B. Tufan, M. Pompe, A. Scavniçar, D. Koçar, Eur. Food Res. Technol. **235**, 669 (2012)
20. V. Šimat, P. Dalgaard, LWT Food Sci. Technol. **44**, 399 (2011)
21. X.-F. Chen, X.-X. Xia, S.Y. Lee, Z.-G. Qian, Biotechnol. Bioeng. **115**, 1014 (2017)
22. X. Ying, H.-T. Yoshioka, C. Liu, F. Sassa, K. Hayashi, Sens. Actuators B Chem. **258**, 870 (2018)
23. C.B. Nielsen, Turbiez Mathieu, and McCulloch Iain. Adv. Mater. **25**, 1859 (2012)
24. B. Nketia-Yawson, Y.-Y. Noh, Macromol. Res. **25**, 489 (2017)
25. G.-S. Ryu, B. Nketia-Yawson, E.-Y. Choi, Y.-Y. Noh, Org. Electron. **51**, 264 (2017)
26. J.S. Ha, K.H. Kim, D.H. Choi, J. Am. Chem. Soc. **133**, 10364 (2011)
27. Z. Chen, M.J. Lee, R. Shahid Ashraf, Y. Gu, S. Albert-Seifried, M. Meedom Nielsen, B. Schroeder, T.D. Anthopoulos, M. Heeney, I. McCulloch, H. Sirringhaus, Adv. Mater. **24**, 647 (2011)
28. F.V. Di Girolamo, C. Aruta, M. Barra, P. D'Angelo, A. Cassinese, Appl. Phys. A **96**, 481 (2009)
29. M. Nikolka, I. Nasrallah, B. Rose, M.K. Ravva, K. Broch, A. Sadhanala, D. Harkin, J. Charmet, M. Hurhangee, A. Brown, S. Illig, P. Too, J. Jongman, I. McCulloch, J.-L. Bredas, H. Sirringhaus, Nat. Mater. **16**, 356 (2017)
30. S.K. Park, D.A. Mourey, J.-I. Han, J.E. Anthony, T.N. Jackson, Org. Electron. **10**, 486 (2009)
31. Y. Hu, X. Ma, Y. Zhang, Y. Che, J. Zhao, ACS Sens. **1**, 22 (2016)
32. A. Lv, Y. Pan, L. Chi, Sensors **17**, 213 (2017)
33. P.K. Sahu, M. Pandey, C. Kumar, S.S. Pandey, W. Takashima, V.N. Mishra, R. Prakash, Sens. Actuators B Chem. **246**, 243 (2017)
34. L.M. Dumitru, K. Manoli, M. Magliulo, G. Palazzo, L. Torsi, Microelectron. J. **45**, 1679 (2014)
35. W. Wang, J. Han, J. Ying, L. Xiang, W. Xie, Org. Electron. **15**, 2568 (2014)
36. M. Kano, T. Minari, K. Tsukagoshi, H. Maeda, Appl. Phys. Lett. **98**, 073307 (2011)